

The Analysis and the Performance of the Parallel-Partial Reset Control System

Xinxin Zhang and S. Hassan HosseinNia*

Abstract—Reset controllers have demonstrated their effectiveness in enhancing performance in precision motion systems. To further exploiting the potential of reset controllers, this study introduces a parallel-partial reset control structure. Frequency response analysis is effective for the design and fine-tuning of controllers in industries. However, conducting frequency response analysis for reset control systems poses challenges due to their nonlinearities. We develop frequency response analysis methods for both the open-loop and closed-loop parallel-partial reset systems. Simulation results validate the accuracy of the analysis methods, showcasing precision enhancements exceeding 100% compared to the traditional describing function method. Furthermore, we design a parallel-partial reset controller within the Proportional–Integral–Derivative (PID) control structure for a mass-spring-damper system. The frequency response analysis of the designed system indicates that, while maintaining the same bandwidth and phase margin of the first-order harmonics, the new system exhibits lower magnitudes of higher-order harmonics, compared to the traditional reset system. Moreover, simulation results demonstrate that the new system achieves lower overshoot and quicker settling time compared to both the traditional reset and linear systems.

I. INTRODUCTION

Reset controllers have demonstrated their ability to overcome the phase-gain limitation and waterbed effects inherent in linear control systems [1]. The first reset element, known as the Clegg Integrator [2], exhibits the same gain characteristic as the linear integrator. However, it offers a 52° phase lead, as determined by describing function analysis. This property enables reset controllers to exhibit superior tracking and disturbance rejection benefits compared to their linear counterparts in various applications, including semiconductor manufacturing, chemical processes, and precision motion systems [1], [3], [4], [5], [6], [7].

Nevertheless, it is essential to acknowledge that reset control, while overcoming linear trade-offs, introduces higher-order harmonics due to its inherent nonlinearity, which can lead to undesirable performance, such as the limit cycle [8]. To mitigate the excessive influence of nonlinearity, various forms of reset controllers, such as partial reset controllers [8] and the “Proportional-Integrator + Clegg Integrator (PI+CI)” configuration [9], have been developed. To the best of our knowledge, the combination of linear and reset elements in parallel configuration is primarily explored within the context

of the “PI+CI” system. There remains significant potential to explore this structure’s applicability with general reset elements.

Frequency response analysis is used to examine the phase and gain properties of a control system to sinusoidal inputs across various frequencies. It serves as an effective tool for engineers to design and fine-tune controllers to meet specific performance requirements in industrial applications. For designing and implementing the “PI+CI” control system in the frequency domain, frequency response analysis is needed. Currently, classical Describing Function (DF) analysis is commonly utilized to analyze such the open-loop “PI+CI” control system. However, DF analysis typically only considers the first-order harmonic, which will lead to analytical inaccuracies. Moreover, there is an absence of precise frequency response analysis methods tailored for closed-loop “PI+CI” systems.

Addressing these gaps in research motivation, this paper makes the following contributions:

- We introduce a novel control system structure termed Parallel-Partial-Reset Control Systems (PP-RCSs), which expands upon the conventional parallel “PI+CI” configuration to accommodate a wider variety of reset control systems.
- A Higher-Order Sinusoidal Input Describing Function (HOSIDF) to analyze the frequency response of open-loop and closed-loop PP-RCSs to sinusoidal reference inputs is developed, building upon our previous research for the traditional reset system.
- We design a PP-RCS for a mass-spring-damper system. The frequency response analysis shows that the PP-RCS significantly reduces the magnitudes of higher-order harmonics in the traditional reset system. Additionally, the PP-RCS exhibits superior transient response compared to traditional reset and linear systems.

This paper is structured into six sections. In Section II, fundamental background of reset systems are provided. Section III outlines the research problems addressed. Section IV elaborates on the frequency-domain analysis of PP-RCS, covering scenarios from open-loop to closed-loop. Simulation results illustrate a substantial accuracy improvement of the new analysis method compared to the DF method. In Section VI, a PP-RCS is designed on a precision motion stage. Simulations highlight the better performance achieved by PP-RCSs compared to traditional reset control systems. Finally, the key findings of this paper are summarized, and future research prospects are outlined in Section VI.

* Corresponding Author.

This work was not supported by any organization.

Xinxin Zhang and S. Hassan HosseinNia are with the Department of Precision and Microsystems Engineering (PME), Delft University of Technology, Mekelweg 2, 2828 CD, Delft, The Netherlands, with Emails: X.Zhang-15@tudelft.nl, S.H.HosseinNiaKani@tudelft.nl.

II. BACKGROUND

A. Definition of the Reset Controller

Figure 1 depicts the block diagram of a closed-loop reset system, comprising a reset controller denoted as \mathcal{C} , a linear controller \mathcal{C}_2 , and a plant \mathcal{P} . The signals $r(t)$, $e(t)$, $u(t)$, and $y(t)$ are the reference input, error, control input, and system output signals respectively.

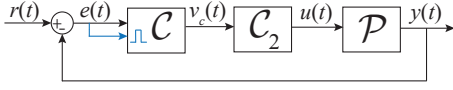


Fig. 1: The block diagram of the RCS, where the blue lines represent the reset action.

The reset controller \mathcal{C} is a linear time-invariant (LTI) system encompassing with a reset mechanism, which is triggered by the input signal $e(t)$. The state-space representative for the \mathcal{C} is described as below:

$$\mathcal{C} = \begin{cases} \dot{x}_r(t) = A_R x_r(t) + B_R e(t), & t \notin J \\ x_r(t^+) = A_\rho I x_r(t), & t \in J \\ v_c(t) = C_R x_r(t) + D_R e(t), \end{cases} \quad (1)$$

where $x_r(t) \in \mathbb{R}^{n_c}$ is the state of the RC and n_c is the number of the states of the RC. A_R , B_R , C_R , D_R are the state-space matrices of the base linear controller denoted as \mathcal{C}_{bl} , given by

$$\mathcal{C}_{bl}(\omega) = C_R(j\omega I - A_R)^{-1} B_R + D_R, \quad (j = \sqrt{-1}). \quad (2)$$

The reset controller \mathcal{C} employs the ‘‘zero-crossing law’’ as its reset mechanism, resetting specific states of \mathcal{C} to zero when the reset triggered signal $e(t)$ crosses zero [8], [10]. At the reset instant $t_i (i \in \mathbb{Z}^+)$, the reset action is activated when $e(t_i) = 0$. The set of reset instants t_i is denoted as $J := \{t_i | e(t_i) = 0, i \in \mathbb{Z}^+\}$. The second equation describes the jump of the state x_r from t_i to t_i^+ . A_ρ represents the reset matrix, defined as:

$$A_\rho = \begin{bmatrix} A_{\rho\gamma} & \\ & I_{n_l} \end{bmatrix}, \quad A_{\rho\gamma} = \text{diag}(\gamma_1, \gamma_2, \dots, \gamma_o, \dots, \gamma_{n_r}). \quad (3)$$

In (3), $\gamma_o \in (-1, 1)$, where $o \in \mathbb{Z}^+$, represents the reset value. The subscript n_r denotes the number of reset states, while n_l indicates the number of linear states, resulting in a total of $n_c = n_r + n_l$. For the scope of this study, our focus lies on reset controllers featuring a single reset state, specifically when $n_r = 1$. Such reset controllers with single reset states are commonly encountered in literature, examples of which include the Clegg Integrator (CI), the First-order Reset Element (FORE) [11], the Second-order Reset Element (SORE) [4] with the reset applied to the first state, etc.

B. Frequency Response Analysis for the Reset Controller

A reset controller (1) with an input signal of $e(t) = |E|\sin(\omega t + \angle E)$ is asymptotically stable with $2\pi/\omega$ -periodic solution and convergent if and only if [12]:

$$|\lambda(D_R e^{A_R \delta})| < 1, \quad \forall \delta \in \mathbb{R}^+. \quad (4)$$

Since the frequency response analysis necessitates system stability and convergence, we introduce the following assumption:

Assumption 1. The reset controller (1) with input $e(t) = |E|\sin(\omega t + \angle E)$ is assumed to meet the condition in (4).

Consider a reset controller \mathcal{C} (1) with input signal $e(t) = |E|\sin(\omega t + \angle E_1)$, satisfying Assumption 1. Utilizing the ‘‘Virtual Harmonic Generator’’ [13], the input signal $e(t)$ generates $n \in \mathbb{N}$ harmonics $e_{1n}(t) = |E|\sin(n\omega t + n\angle E_1)$. There are n harmonics in the output signal $v_c(t)$, given by $v_c(t) = \sum_{n=1}^{\infty} v_c^n(t)$. The function $H_n(\omega)$ represents the transfer function from $e_{1n}(t)$ to $v_c^n(t)$, which is provided in [13], [14] and given by

$$H_n(\omega) = \begin{cases} C_R(j\omega I - A_R)^{-1}(I + j\Theta_D(\omega))B_R + D_R, & \text{for } n = 1 \\ C_R(jn\omega I - A_R)^{-1}j\Theta_D(\omega)B_R, & \text{for odd } n > 1 \\ 0, & \text{for even } n \geq 2 \end{cases} \quad (5)$$

with

$$\begin{aligned} \Lambda(\omega) &= \omega^2 I + A_R^2, \\ \Delta(\omega) &= I + e^{(\frac{\pi}{\omega} A_R)}, \\ \Delta_r(\omega) &= I + A_\rho e^{(\frac{\pi}{\omega} A_R)}, \\ \Gamma_r(\omega) &= \Delta_r^{-1}(\omega) A_\rho \Delta(\omega) \Lambda^{-1}(\omega), \\ \Theta_D(\omega) &= \frac{-2\omega^2}{\pi} \Delta(\omega) [\Gamma_r(\omega) - \Lambda^{-1}(\omega)]. \end{aligned} \quad (6)$$

III. PROBLEM STATEMENT

The block diagram of a Parallel-Partial Reset Control System (PP-RCS) is depicted in Fig. 2. It comprises a control structure \mathcal{H}_p , a linear controller \mathcal{C}_2 , and a plant \mathcal{P} .

The control element \mathcal{H}_p integrates a reset controller \mathcal{C} (1) and its corresponding base-linear controller \mathcal{C}_{bl} (2) configured in parallel, with proportions of k_{rc} and $1 - k_{rc}$, respectively, given by

$$\begin{aligned} \mathcal{H}_p &= \mathcal{H}_{rc} + \mathcal{H}_{bl}, \\ \mathcal{H}_{rc} &= k_{rc} \mathcal{C}, \quad k_{rc} \in [0, 1] \in \mathbb{R}, \\ \mathcal{H}_{bl} &= (1 - k_{rc}) \mathcal{C}_{bl}. \end{aligned} \quad (7)$$

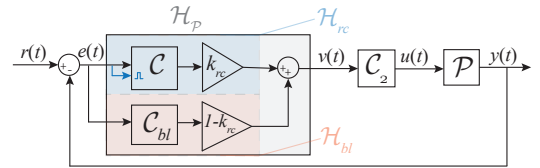


Fig. 2: The block diagram of the PP-RCS, where $r(t)$, $e(t)$, $v(t)$, $u(t)$, and $y(t)$ are the reference input, error, reset output, control input, and system output signals respectively. The blue lines represent the reset action.

The objective of this research is to develop a methodology for analyzing the frequency response of the PP-RCS to sinusoidal inputs, encompassing both its phase and gain characteristics across various frequencies. This analysis aims to provide insights into the steady-state behavior of the

system and serve as a tool for designing the PP-RCS to meet specific specifications.

Let the set \mathcal{L}_2 consists of all measurable functions $f(\cdot) : \mathbb{R}_+ \rightarrow \mathbb{R}$ such that $\int_0^\infty |f(t)|^2 dt < \infty$, being the \mathcal{L}_2 -norm $\|\cdot\| : \mathcal{L}_2 \rightarrow \mathbb{R}_+$ defined by $\|f\| = \sqrt{\int_0^\infty |f(t)|^2 dt}$.

Note that the stability and convergence for reset systems can be ensured through thorough design practices, which are not the primary focus of this research. However, to ensure the existence of the frequency response of the closed-loop reset system, the following assumption is made to guarantee stability [15] and convergence [16] of the closed-loop reset system:

Assumption 2. The closed-loop PP-RCS is assumed to be \mathcal{L}_2 -stable, the initial condition of the reset controller \mathcal{C} is zero, there are infinitely many reset instants t_i with $\lim_{t_i \rightarrow \infty} = \infty$, the input signal $r(t) = |R|\sin(\omega t)$ is a Bohl function [17], and there is no Zenoness behaviour.

Under Assumption 2, as per [18], in Fig. 2, $e(t)$, $v(t)$, $u(t)$, and $y(t)$ are periodic signals with the same fundamental frequency as $r(t)$ and can be expressed as follows:

$$e(t) = \sum_{n=1}^{\infty} e_n(t) = \sum_{n=1}^{\infty} |E_n| \sin(n\omega t + \angle E_n), \quad (8)$$

where $\angle E_n \in (-\pi, \pi]$. The Fourier transform of $e_n(t)$ is $E_n(\omega) = \mathcal{F}[e_n(t)]$.

The closed-loop reset systems under a sinusoidal input with more than two reset instants possess excessive higher-order harmonics compared to systems with only two reset instants [14]. However, such effects can be mitigated through careful design considerations [19]. Moreover, practical reset control systems commonly employ systems with two reset instants [8]. Building on these observations, we introduce the following assumption:

Assumption 3. There are two reset instants in a SISO closed-loop PP-RCS with a sinusoidal reference input signal $r(t) = |R|\sin(\omega t)$ at steady-state, where the reset-triggered signal is $e_1(t)$.

Under Assumptions 2 and 3, the reset actions in the closed-loop SISO PP-RCS to the sinusoidal input $r(t) = |R|\sin(\omega t)$ occur when $e_1(t) = |E_1|\sin(\omega t + \angle E_1) = 0$. The set of reset instants for this closed-loop reset system is denoted as $J_m := \{t_m = (m\pi - \angle E_1)/\omega | m \in \mathbb{Z}^+\}$.

Consider a SISO PP-RCS with $k_{rc} = 1$, subjected to a reference input signal $r(t) = |R|\sin(\omega t)$, and under Assumptions 2 and 3.

From (5), The n -th open-loop transfer function of the PP-RCS with $k_{rc} = 1$ denoted as \mathcal{L}_n is given by

$$\mathcal{L}_n(\omega) = H_n(\omega) \mathcal{C}_2(n\omega) \mathcal{P}(n\omega). \quad (9)$$

Define

$$\begin{aligned} \mathcal{C}_{nl}(\omega) &= H_1(\omega) - \mathcal{C}_{bl}(\omega), \\ \mathcal{C}_{nl}(n\omega) &= H_n(\omega), \text{ for } n > 1. \end{aligned} \quad (10)$$

Then, the open-loop transfer function of the PP-RCS with $k_{rc} = 1$ in (9) is separated into linear and nonlinear elements,

given by:

$$\begin{aligned} \mathcal{L}_{bl}(n\omega) &= \mathcal{C}_{bl}(n\omega) \mathcal{C}_2(n\omega) \mathcal{P}(n\omega), \\ \mathcal{L}_{nl}(n\omega) &= \mathcal{C}_{nl}(n\omega) \mathcal{C}_2(n\omega) \mathcal{P}(n\omega), \\ \mathcal{C}_{nl}(n\omega) &= C_R(jn\omega I - A_R)^{-1} j \Theta_D(\omega) B_R. \end{aligned} \quad (11)$$

Utilizing the ‘‘Virtual Harmonic Generator,’’ the input signal $r(t)$ generates n harmonics $r_n(t) = |R|\sin(n\omega t)$, with $R_n(\omega) = \mathcal{F}[r_n(t)]$. In our previous research [20], we derived the n^{th} sensitivity function $\mathcal{S}_n(\omega)$ for the PP-RCS with $k_{rc} = 1$. It is defined as $\mathcal{S}_n(\omega) = E_n(\omega)/R_n(\omega)$ and can be obtained from the open-loop transfer functions in (11), given by:

$$\mathcal{S}_n(\omega) = \begin{cases} \frac{1}{1 + \mathcal{L}_o(\omega)}, & \text{for } n = 1 \\ -\frac{\Gamma(\omega) \mathcal{L}_{nl}(n\omega) |\mathcal{S}_1(\omega)| e^{jn \angle \mathcal{S}_1(\omega)}}{1 + \mathcal{L}_{bl}(n\omega)}, & \text{for odd } n > 1 \\ 0, & \text{for even } n \geq 2 \end{cases} \quad (12)$$

where

$$\begin{aligned} \Delta_l(n\omega) &= (jn\omega I - A_R)^{-1} B_R, \\ \Delta_c(\omega) &= |\Delta_l(\omega)| \sin(\angle \Delta_l(\omega)), \\ \mathcal{L}_o(n\omega) &= \mathcal{L}_{bl}(n\omega) + \Gamma(\omega) \mathcal{L}_{nl}(n\omega), \\ \Psi_n(\omega) &= |\mathcal{L}_{nl}(n\omega)| / |1 + \mathcal{L}_{bl}(n\omega)|, \\ \Gamma(\omega) &= 1 / [1 - \sum_{n=3}^{\infty} \Psi_n(\omega) \Delta_c^n(\omega) / \Delta_c(\omega)], \\ \Delta_c^n(\omega) &= -|\Delta_l(n\omega)| \sin(\angle \mathcal{L}_{nl}(n\omega) - \angle(1 + \mathcal{L}_{bl}(n\omega)) + \angle \Delta_l(n\omega)). \end{aligned} \quad (13)$$

The frequency response analysis for the PP-RCS with $k_{rc} \in [0, 1]$ is presented in Section IV.

IV. FREQUENCY RESPONSE ANALYSIS FOR THE PARALLEL-PARTIAL RESET CONTROL SYSTEM

In this section, Theorem 1 and Corollary 1 propose the Higher-order sinusoidal input describing function (HOSIDF) for open-loop and closed-loop PP-RCSs, respectively.

A. Frequency Response Analysis for the Open-loop and Closed-loop PP-RCS

Consider a parallel-partial reset controller (PP-RC) \mathcal{H}_p as depicted in Fig. 2, operating under the sinusoidal input signal $e_1(t) = |E_1|\sin(\omega t + \angle E_1)$, where $\angle E_1 \in [-\pi, \pi)$, and under the Assumption 1. The steady-state output signal of \mathcal{H}_p is denoted as $v_1(t)$, which comprises $n \in \mathbb{N}$ harmonics, represented as $v_1(t) = \sum_{n=1}^{\infty} v_{1n}(t)$. The block diagram of \mathcal{H}_p is illustrated in Fig. 3. By utilizing the ‘‘Virtual Harmonic Generator’’ [14], the input signal $e_1(t)$ generates n harmonics, denoted as $e_{1n}(t) = |E_1|\sin(n\omega t + n\angle E_1)$.

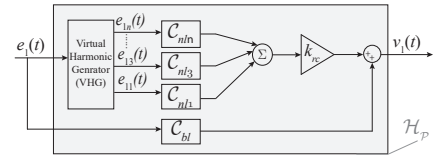


Fig. 3: The block diagram of the parallel-partial reset controller (PP-RC) \mathcal{H}_p .

Theorem 1. (Frequency Response Analysis for the Open-loop PP-RCS) The n -th Higher-order sinusoidal input describing function (HOSIDF) for \mathcal{H}_p , defined as $H_p^n(\omega)$, represents the transfer function from $E_{1n}(\omega) = \mathcal{F}[e_{1n}(t)]$ to $V_{1n}(\omega) = \mathcal{F}[v_{1n}(t)]$, and is given by:

$$H_p^n(\omega) = \frac{V_{1n}(\omega)}{E_{1n}(\omega)} = \begin{cases} C_{bl}(\omega) + k_{rc}C_{nl}(\omega), & \text{for } n = 1 \\ k_{rc}C_{nl}(n\omega), & \text{for odd } n > 1 \\ 0, & \text{for even } n \geq 2 \end{cases} \quad (14)$$

where $C_{bl}(\omega)$ is given in (2) and $C_{nl}(n\omega)$ is given in (11).

Proof. From (7) and (10), the n -th HOSIDF for \mathcal{H}_{rc} is defined as

$$\mathcal{H}_{rc}^n(\omega) = \begin{cases} k_{rc}C_{bl}(\omega) + k_{rc}C_{nl}(\omega), & \text{for } n = 1 \\ k_{rc}C_{nl}(n\omega), & \text{for odd } n > 1 \\ 0, & \text{for even } n \geq 2. \end{cases} \quad (15)$$

The transfer function for \mathcal{H}_{bl} is defined as

$$\mathcal{H}_{bl}(\omega) = (1 - k_{rc})C_{bl}(\omega). \quad (16)$$

From (15), (16), and the definition of \mathcal{H}_p in (7), the first-order harmonic of \mathcal{H}_p denoted as $\mathcal{H}_p^1(\omega)$ is given by

$$\begin{aligned} \mathcal{H}_p^1(\omega) &= \mathcal{H}_{rc}^1(\omega) + \mathcal{H}_{bl}^1(\omega) \\ &= C_{bl}(\omega) + k_{rc}C_{nl}(\omega). \end{aligned} \quad (17)$$

The higher-order harmonics $n = 2k + 1 > 1$, $k \in \mathbb{N}$ of \mathcal{H}_p denoted as $\mathcal{H}_p^n(\omega)$ is given by

$$\mathcal{H}_p^n(\omega) = k_{rc}C_{nl}(n\omega). \quad (18)$$

Combining (17) and (18), the proof is concluded. \square

Remark 1. Compared to the HOSIDF for the traditional reset controller \mathcal{H}_p with $k_{rc} = 1$ in (5), the HOSIDF for \mathcal{H}_p in (14) introduces a new parameter k_{rc} to adjust the nonlinearity $C_{nl}(n\omega)$ (11) of the reset controller \mathcal{C} , while maintaining the linear element $C_{bl}(\omega)$ (2) in \mathcal{C} unchanged.

Corollary 1. (Frequency Response Analysis for the Closed-loop PP-RCS) Consider a SISO PP-RCS, as illustrated in Fig. 2, which receives a sinusoidal input signal $r(t) = |R|\sin(\omega t)$, under Assumptions stated in 2 and 3. The n^{th} sensitivity function $S_n(\omega) = E_n(\omega)/R_n(\omega)$ is defined as

$$S_n(\omega) = \begin{cases} \frac{1}{1 + \mathcal{L}_o(\omega)}, & \text{for } n = 1 \\ -\frac{\Gamma(\omega)\mathcal{L}_{nl}(n\omega)|S_1(\omega)|e^{jn\angle S_1(\omega)}}{1 + \mathcal{L}_{bl}(n\omega)}, & \text{for odd } n > 1 \\ 0, & \text{for even } n \geq 2 \end{cases} \quad (19)$$

where

$$\begin{aligned} \mathcal{L}_{bl}(n\omega) &= C_{bl}(n\omega)\mathcal{C}_2(n\omega)\mathcal{P}(n\omega), \\ \mathcal{L}_{nl}(n\omega) &= k_{rc}C_{nl}(n\omega)\mathcal{C}_2(n\omega)\mathcal{P}(n\omega), \end{aligned} \quad (20)$$

Functions $C_{bl}(\omega)$, $C_{nl}(\omega)$, and $\Gamma(\omega)$ are given in (2) and (20).

Proof. As illustrated in Theorem 1, the HOSIDF of a PP-RCS is divided into linear element $C_{bl}(\omega)$ and nonlinear element

$k_{rc}C_{nl}(n\omega)$. The HOSIDF of the open-loop PP-RCS is then given by

$$\mathcal{L}_n(\omega) = \begin{cases} k_{rc}C_{bl}(\omega) + k_{rc}C_{nl}(\omega), & \text{for } n = 1 \\ k_{rc}C_{nl}(n\omega), & \text{for odd } n > 1 \\ 0, & \text{for even } n \geq 2 \end{cases} \quad (21)$$

where

$$\begin{aligned} \mathcal{L}_{bl}(n\omega) &= C_{bl}(n\omega)\mathcal{C}_2(n\omega)\mathcal{P}(n\omega), \\ \mathcal{L}_{nl}(n\omega) &= K_{rc}C_{nl}(n\omega)\mathcal{C}_2(n\omega)\mathcal{P}(n\omega). \end{aligned} \quad (22)$$

By replacing the open-loop transfer functions for the PP-RCS from (11) with the new functions (22), and substituting them into the closed-loop sensitivity function (12), the proof is concluded. \square

Remark 2. Consider a SISO PP-RCS, as illustrated in Fig. 2, which receives a sinusoidal input signal $r(t) = |R|\sin(\omega t)$, under the assumptions stated in 2 and 3. The steady-state error signal $e(t)$ predicted by the DF in [12] is defined as

$$e(t) = \mathcal{F}^{-1}[R_1(\omega)/(1 + H_1(\omega))]. \quad (23)$$

The steady-state error signal $e(t)$ predicted by the HOSIDF in Corollary 1 is defined as

$$e(t) = \sum_{n=1}^{\infty} \mathcal{F}^{-1}[S_n(\omega)R_n(\omega)]. \quad (24)$$

Due to the nonlinearity inherent in the reset system, the error signal $e(t)$ comprises an infinite number of harmonics. Equation (23) only addresses the first-order harmonic, whereas equation (24) encompasses higher-order harmonics (for $n > 1$). This inclusion results in improved prediction accuracy, as demonstrated in Subsection IV-B.

B. Illustrative Example: The Accuracy of the Analysis Method for the PP-RCS

We employ a mass-spring-damper system (which is a one-degree precision motion stage shown in [19]) as the plant \mathcal{P} , whose transfer function is given by:

$$\mathcal{P}(s) = \frac{6.615e5}{83.57s^2 + 279.4s + 5.837e5}. \quad (25)$$

The Proportional-Clegg-Integrator (PCI) controller is built by replacing the integrator in the Proportional-Integrator (PI) controller with the Clegg Integrator (CI). We have constructed a Parallel-Partial PCI-PID (PP-PCI-PID) controller, implemented on $\mathcal{P}(s)$ as depicted in Fig. 4. The integral frequency in the PCI controller is set to $\omega_i = 2\pi \cdot 15$ rad/s, with the proportional gain value $k_{rc} = 0.7$, and the reset value $\gamma = -0.5$. The parameters in the PID structure are chosen to achieve a bandwidth of 150 Hz and a phase margin of 50° in open-loop.

Figure 5 compares the simulated, equation (24)(HOSIDF)-predicted, and the equation (23)(DF)-predicted steady-state error $e(t)$ on the PP-PCI-PID system with a sinusoidal input signal $r(t) = \sin(2\pi ft)$, ($\omega = 2\pi f$) at the input frequencies f of 100 Hz, 1000 Hz, and 20 Hz. From the comparison, two key conclusions can be drawn:

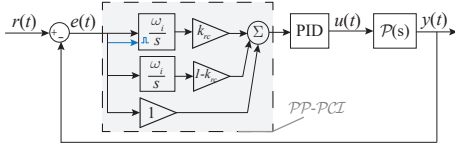


Fig. 4: The PP-PCI-PID control system structure.

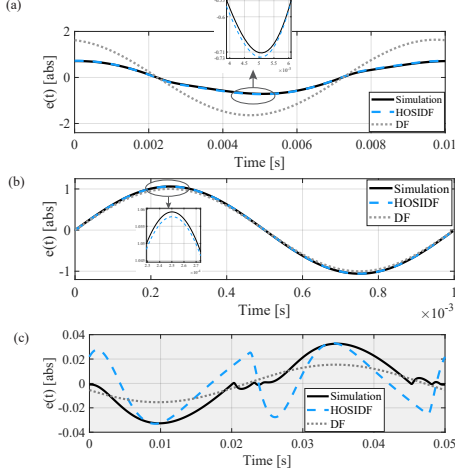


Fig. 5: The steady-state error $e(t)$ of the PP-PCI-PID system at input frequencies of (a) $f = 100$ Hz, (b) $f = 1000$ Hz, and (c) $f = 20$ Hz, obtained from simulation, HOSIDF analysis (24), and DF analysis (23).

(1) Figure 5(a) and (b) show that the new HOSIDF method accurately predicts the steady-state error signal of the closed-loop PP-PCI-PID system. There’s a significant improvement in accuracy achieved by the HOSIDF analysis compared to the DF analysis, which exceeds 100% at an input frequency of 100 Hz. The enhanced precision of the new HOSIDF over the DF results from the HOSIDF method incorporating higher-order harmonics into the analysis, whereas the DF method only considers the first-order harmonic in the calculation process, in line with Remark 2.

(2) However, in Fig. 5(c), the HOSIDF inaccurately predicts the steady-state error of the system at 20 Hz due to the violation of Assumption 3. In practical design, it’s desirable to adhere to Assumption 3 and avoid scenarios with multiple reset instances, as they introduce excessive higher-order harmonics. We apply this example to show that in cases where Assumption 3 is not valid, the reliability of the HOSIDF analysis is compromised.

V. THE PERFORMANCE OF THE PP-RCS

A. The PP-CgLp-PI²D control system

The reset component “Constant in Gain Lead in Phase” (CgLp) provides phase lead without compromising gain advantages [6]. We constructed a Parallel-Partial CgLp-PI²D (PP-CgLp-PI²D) control system, as illustrated in Fig. 6, where PI²D is the PID controller with an additional integrator. The parameter $\omega_c = 2\pi \cdot 150$ rad/s is utilized. The PI²D is configured to achieve a bandwidth of 150 Hz and

a phase margin of 50° in open-loop. The transfer function $\mathcal{P}(s)$ is defined in (25).

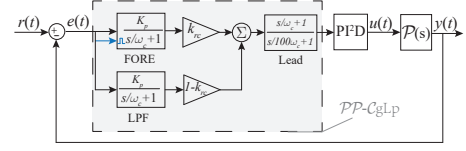


Fig. 6: The PP-CgLp-PI²D control system structure.

Three reset systems denoted as C_1 , C_2 , and C_3 within the PP-CgLp-PI²D system structure were designed, each with different pairs of (γ, k_{rc}) values. The (γ, k_{rc}) parameters for C_1 - C_3 are specified as follows: Linear system C_1 : $(\gamma, k_{rc})=(1, 1)$, traditional reset system C_2 : $(\gamma, k_{rc})=(-0.5, 1)$, and new PP-RCS C_3 : $(\gamma, k_{rc})=(-0.5, 0.5)$. We maintain the same bandwidth of 150 Hz and phase margin of 50° in the first-order harmonic for the open-loop systems C_1 - C_3 . These three systems under a sinusoidal input signal have approximately two reset instants per steady-state cycle across the entire frequency range, thereby satisfying Assumption 3. Additionally, they have been verified to be stable and convergent, meeting Assumption 2.

B. Open-loop Analysis for Systems C_1 - C_3

Figure 7 illustrates the open-loop HOSIDF $H_p^n(\omega)$ for $n = 1$ and $n = 3$ in C_1 - C_3 . For the first-order harmonics, despite maintaining the same phase margin and bandwidth, the reset control system C_2 exhibits slightly larger magnitudes of the first-order harmonics at low frequencies compared to systems C_1 and C_3 . Concerning the higher-order harmonics, system C_3 demonstrates lower magnitudes of higher-order harmonics compared to C_2 .

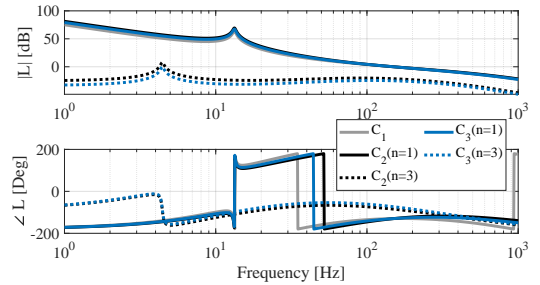


Fig. 7: The HOSIDF $H_p^n(\omega)$ for $n = 1$ and $n = 3$ in open-loop systems C_1 - C_3 .

C. Closed-loop Analysis for Systems C_1 - C_3

Figure 8(a) and (b) illustrate the \mathcal{L}_2 (root mean square $\|e\|_2$) and \mathcal{L}_∞ ($\|e\|_\infty$) norms of the steady-state errors in systems C_1 - C_3 , predicted by Corollary 1. Compared to the traditional reset system C_2 , system C_3 exhibits similar performance at low frequencies, achieves better tracking at mid frequencies (ranging from 80 Hz to 150 Hz), with a marginal compromise at high frequencies. Figure 8(c) and (d)

show the simulated steady-state errors at input frequencies of 1 Hz and 100 Hz, validating the prediction results in Fig. 8(a) and (b).

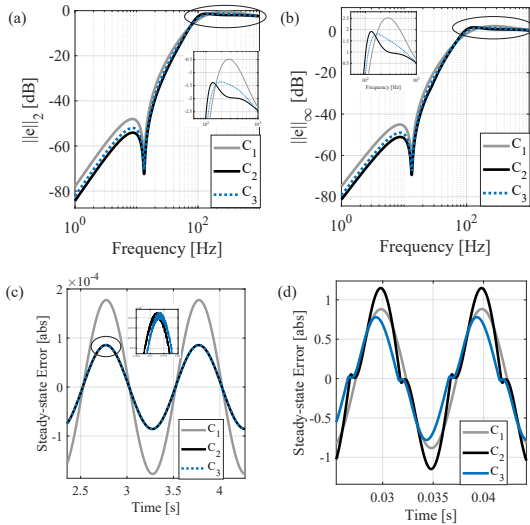


Fig. 8: (a) The \mathcal{L}_2 and (b) the \mathcal{L}_∞ norms of steady-state errors in systems C_1 - C_3 . The simulated steady-state errors in C_1 - C_3 at input frequencies of (c) 1 Hz and (d) 100 Hz.

D. Transient Responses for Systems C_1 - C_3 and Future Work

Figure 9 illustrates the step responses of these three systems. While reset system C_2 exhibits lower overshoot compared to the linear system C_1 , it sacrifices settling time. System C_3 achieves the lowest overshoot while maintaining a similar settling time to the linear system C_1 . The lower overshoot compared to system C_2 may be attributed to the fact that in open-loop, the magnitudes of higher-order harmonics of C_3 are lower, and in closed-loop, the maximum steady-state error of system C_3 is lower (as shown in Fig. 8(b)). Further exploration of the analytical relationship between the transient response and frequency domain analysis is warranted in future research.

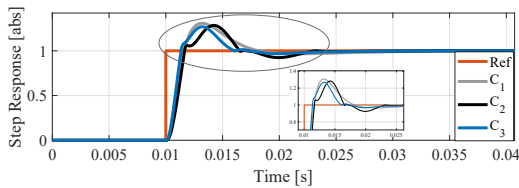


Fig. 9: The step responses for systems C_1 - C_3 .

VI. CONCLUSION

This study introduces a PP-RCS structure, which incorporates a new parameter k_{rc} to adjust the nonlinearity of the reset system while keeping the linearity unchanged. To facilitate effective design in the frequency domain, this work presents frequency response analysis methods for both open-loop and closed-loop PP-RCSs. Simulation results show the enhanced accuracy achieved by the new analysis methods

compared to the traditional DF method. An illustrative example on a mass-spring-damper system illustrates the improved transient responses of the PP-RCS compared to traditional reset and linear systems. For future work, experimental validation is warranted. Additionally, it is worthwhile to explore the relation between the transient responses of the PP-RCS and its frequency domain properties.

REFERENCES

- [1] Linda Chen, Niranjan Saikumar, and S Hassan HosseinNia. Development of robust fractional-order reset control. *IEEE Transactions on Control Systems Technology*, 28(4):1404–1417, 2019.
- [2] John C Clegg. A nonlinear integrator for servomechanisms. *Transactions of the American Institute of Electrical Engineers, Part II: Applications and Industry*, 77(1):41–42, 1958.
- [3] Yuhang Zheng, Y Chait, CV Hollot, M Steinbuch, and M Norg. Experimental demonstration of reset control design. *Control Engineering Practice*, 8(2):113–120, 2000.
- [4] Leroy Hazeleger, Marcel Heertjes, and Henk Nijmeijer. Second-order reset elements for stage control design. In *2016 American Control Conference (ACC)*, pages 2643–2648. IEEE, 2016.
- [5] Justin H Le and Andrew R Teel. Passive soft-reset controllers for nonlinear systems. In *2021 60th IEEE conference on decision and control (CDC)*, pages 5320–5325. IEEE, 2021.
- [6] Niranjan Saikumar, Rahul Kumar Sinha, and S Hassan HosseinNia. “constant in gain lead in phase” element–application in precision motion control. *IEEE/ASME Transactions on Mechatronics*, 24(3):1176–1185, 2019.
- [7] Arun Palanikumar, Niranjan Saikumar, and S Hassan HosseinNia. No more differentiator in pid: Development of nonlinear lead for precision mechatronics. In *2018 european control conference (ECC)*, pages 991–996. IEEE, 2018.
- [8] Alfonso Banos and Antonio Barreiro. *Reset control systems*. Springer, 2012.
- [9] Alfonso Baños and Angel Vidal. Definition and tuning of a pi+ ci reset controller. In *2007 european control conference (ECC)*, pages 4792–4798. IEEE, 2007.
- [10] Ying Li, Guoxiao Guo, and Youyi Wang. Reset control for mid-frequency narrowband disturbance rejection with an application in hard disk drives. *IEEE Transactions on Control Systems Technology*, 19(6):1339–1348, 2010.
- [11] Isaac Horowitz and Patrick Rosenbaum. Non-linear design for cost of feedback reduction in systems with large parameter uncertainty. *International Journal of Control*, 21(6):977–1001, 1975.
- [12] Yuqian Guo, Youyi Wang, and Lihua Xie. Frequency-domain properties of reset systems with application in hard-disk-drive systems. *IEEE Transactions on Control Systems Technology*, 17(6):1446–1453, 2009.
- [13] Kars Heinen. Frequency analysis of reset systems containing a clegg integrator: An introduction to higher order sinusoidal input describing functions. 2018.
- [14] Niranjan Saikumar, Kars Heinen, and S Hassan HosseinNia. Loop-shaping for reset control systems: A higher-order sinusoidal-input describing functions approach. *Control Engineering Practice*, 111:104808, 2021.
- [15] Orhan Beker, CV Hollot, Yossi Chait, and Huaizhong Han. Fundamental properties of reset control systems. *Automatica*, 40(6):905–915, 2004.
- [16] Ali Ahmadi Dastjerdi, Alessandro Astolfi, and S Hassan HosseinNia. A frequency-domain stability method for reset systems. In *2020 59th IEEE Conference on Decision and Control (CDC)*, pages 5785–5791. IEEE, 2020.
- [17] EA Barabanov and AV Konyukh. Bohl exponents of linear differential systems. *Mem. Differential Equations Math. Phys.*, 24:151–158, 2001.
- [18] Alexey Pavlov, Nathan Van De Wouw, and Hendrik Nijmeijer. *Uniform output regulation of nonlinear systems: a convergent dynamics approach*, volume 205. Springer, 2006.
- [19] Nima Karbasizadeh, Ali Ahmadi Dastjerdi, Niranjan Saikumar, and S Hassan HosseinNia. Band-passing nonlinearity in reset elements. *IEEE Transactions on Control Systems Technology*, 31(1):333–343, 2022.
- [20] Xinxin Zhang, Marcin B Kaczmarek, and S Hassan HosseinNia. Frequency-domain analysis for reset systems using pulse-based model. *arXiv preprint arXiv:2206.00523*, 2022.